THE JOURNAL OF BIOLOGICAL CHEMISTRY
Vol. 279, No. 34, Issue of August 20, pp. 36029–36037, 2004
Printed in U.S.A.
© 2004 by The American Society for Biochemistry and Molecular Biology, Inc.

# The Dual Nature of the Wheat Xylanase Protein Inhibitor XIP-I

STRUCTURAL BASIS FOR THE INHIBITION OF FAMILY 10 AND FAMILY 11 XYLANASES*[S]

Received for publication, April 16, 2004, and in revised form, May 27, 2004
Published, JBC Papers in Press, June 4, 2004, DOI 10.1074/jbc.M404225200

**Françoise Payan‡, Philippe Leone‡, Sophie Porciero‡, Caroline Furniss§, Tariq Tahir§, Gary Williamson§¶, Anne Durand§, Paloma Manzanares‖, Harry J. Gilbert**, Nathalie Juge§‡‡§§, and Alain Roussel‡**

*From the ‡Architecture et Fonction de Macromolécules Biologiques, UMR-6098, CNRS et Universités d'Aix-Marseille I et II, 31 Chemin Joseph Aiguier, 13402 Marseille Cedex 20, France, §Institute of Food Research, Colney Lane, Norwich NR4 7UA, United Kingdom, ‖Instituto de Agroquímica y Tecnología de Alimentos, CSIC, P. O. Box 73, 46100 Burjassot, Valencia, Spain, **School of Cell and Molecular Biosciences, University of Newcastle upon Tyne, Newcastle upon Tyne NE1 7RU, United Kingdom, and ‡‡Institut Méditerranéen de Recherche en Nutrition, UMR INRA 1111, Faculté des Sciences et Techniques de St. Jérôme, Avenue Escadrille Normandie Niemen, F-13397 Marseille, France*

**The xylanase inhibitor protein I (XIP-I) from wheat *Triticum aestivum* is the prototype of a novel class of cereal protein inhibitors that inhibit fungal xylanases belonging to glycoside hydrolase families 10 (GH10) and 11 (GH11). The crystal structures of XIP-I in complex with *Aspergillus nidulans* (GH10) and *Penicillium funiculosum* (GH11) xylanases have been solved at 1.7 and 2.5 Å resolution, respectively. The inhibition strategy is novel because XIP-I possesses two independent enzyme-binding sites, allowing binding to two glycoside hydrolases that display a different fold. Inhibition of the GH11 xylanase is mediated by the insertion of an XIP-I Π-shaped loop (L$\alpha_4\beta_5$) into the enzyme active site, whereas residues in the helix $\alpha$7 of XIP-I, pointing into the four central active site subsites, are mainly responsible for the reversible inactivation of GH10 xylanases. The XIP-I strategy for inhibition of xylanases involves substrate-mimetic contacts and interactions occluding the active site. The structural determinants of XIP-I specificity demonstrate that the inhibitor is able to interact with GH10 and GH11 xylanases of both fungal and bacterial origin. The biological role of the xylanase inhibitors is discussed in light of the present structural data.**

The enzymatic hydrolysis of the plant cell wall, which comprises the most abundant source of organic carbon in the biosphere, releases organic carbon that is utilized as an energy and carbon source by a range of organisms. This degradative process is thus of fundamental biological and industrial importance. A significant component of the plant cell wall is the $\beta$-1,4-xylopyranose polysaccharide xylan, which is hydrolyzed by endo-$\beta$-1,4-xylanases (xylanases) that belong mainly to glycoside hydrolase families (GHs)[1] 10 and 11 (CAZY website, afmb.cnrs-mrs.fr/CAZY/ (1)). These two families have different structures and catalytic properties (2–4). GH11 enzymes are $\beta$-jelly roll proteins in which the substrate-binding groove is formed by the concave face of one of the $\beta$-sheets (see Ref. 5, for example), whereas GH10 xylanases are $(\beta/\alpha)_8$ barrels with the two catalytic glutamate residues located at the C termini of strands $\beta$4 and $\beta$7 (see Ref. 6, for example). Enzymes from both GH10 and GH11 cleave the glycosidic bond by acid-base assisted catalysis by using a double displacement mechanism in which the two catalytic glutamates function as the nucleophile and acid-base residues, respectively.

Recently, two families of plant proteins, designated as XIP and TAXI, have been shown to inhibit xylanases (7, 8). XIP-I from wheat (*Triticum aestivum*) is the prototype of a novel class of "chitinase-like" cereal inhibitors that apparently inhibits reversibly fungal but not bacterial GH10 and GH11 xylanases (9–11). The crystal structure of XIP-I was recently determined to 1.8 Å resolution (12). The inhibitor has a $(\beta/\alpha)_8$ barrel fold and displays structural features typical of the glycoside hydrolase family 18. Although the catalytic glutamate of GH18 chitinases is conserved in XIP-I, structural differences in the region homologous to the active site of chitinases probably account for the lack of activity of XIP-I toward chitin (12). The inhibition of xylanases by XIP-I is competitive with a 1:1 stoichiometry and, depending on the xylanase, the $K_i$ of the inhibition varies 200-fold (10). XIP-I does not show a preference for GH10 or GH11 xylanases because the two tightest-binding complexes were reported to be with the GH11 *Penicillium funiculosum* ($K_i$ of 3.4 nM) and GH10 *Aspergillus nidulans* ($K_i$ of 9 nM) xylanases (10). Inhibition of fungal xylanases is not due to the binding of XIP-I to *glyco*-decorations, because both the native and *Escherichia coli*-derived recombinant forms of *P. funiculosum* xylanase are inhibited to the same extent. Recent site-directed mutagenesis studies have shown that XIP-I binds to the conserved "thumb" hairpin loop of GH11 xylanases (13); however, the mechanism by which the inhibitor recognizes these structures and how the plant protein interacts with GH10 enzymes is unknown.

* This work was supported by the Commission of the European Communities, specific RTD program "Quality of Life and Management of Living Resources," Key Action 1-Health Food and Environment, Project QLRT-2000–811 GEMINI "Solving the Problem of Glycosidase Inhibitors in Food Processing." The costs of publication of this article were defrayed in part by the payment of page charges. This article must therefore be hereby marked "*advertisement*" in accordance with 18 U.S.C. Section 1734 solely to indicate this fact.

[S] The on-line version of this article (available at http://www.jbc.org) contains Tables 1–3.

*The atomic coordinates and structure factors (codes 1TA3 and 1TE1) have been deposited in the Protein Data Bank, Research Collaboratory for Structural Bioinformatics, Rutgers University, New Brunswick, NJ (http://www.rcsb.org/).*

¶ Present address: Nestlé Research Centre, Vers-Chez-Les-Blanc, P. O. Box 44, CH-1000 Lausanne 26, Switzerland.

§§ To whom correspondence should be addressed. Tel.: 44-1603255068; Fax: 44-1603255038; E-mail: nathalie.juge@bbsrc.ac.uk.

[1] The abbreviations used are: GH, glycoside hydrolase; TAXI, *T. aestivum* xylanase inhibitor; XIP, xylanase inhibitor protein; XLNC, *A. nidulans* xylanase; XYNA, *P. simplicissimum* xylanase; XYNC, *P. funiculosum* xylanase C.



This is an Open Access article under the CC BY license.

Here we report the x-ray structure of XIP-I in complex with an *A. nidulans* GH10 and *P. funiculosum* GH11 xylanases. The structural data provide insights into the biological role of a novel protein. Furthermore, knowledge of the structural basis for xylanase recognition by XIP-I provides a template for engineering novel specificities into both xylanase inhibitors and xylanases that could increase the biotechnological applications of these proteins.

## EXPERIMENTAL PROCEDURES

*Protein Expression and Purification*—XIP-I was purified from wheat flour (*T. aestivum* var. *soisson*) as described previously (9, 10). *A. nidulans* xylanase XLNC and *P. funiculosum* xylanase XYNC were overexpressed (14, 15) and purified as described earlier (10, 11).

*Crystallization and Data Collection*—XIP-I-XLNC complex crystals were obtained by vapor diffusion in hanging drops at 20 °C. The *A. nidulans* xylanase was incubated with the inhibitor in a molar ratio prior to crystallization. The hanging drops consisted of 1 $\mu$l of the protein solution (4.2 mg/ml) together with 1 $\mu$l of the reservoir solution composed of 10% PEG 8000, 0.1 M Hepes, pH 7.5, and 20% ethylene glycol. Crystals, grown for 3–10 days (to a maximum size of 0.15 × 0.15 × 0.5 mm), belonged to the $P2_12_12_1$ space group ($a$ = 46.7 Å, $b$ = 75.8 Å and $c$ = 159.6 Å) and diffracted to 1.7 Å resolution. Ethylene glycol was added up to a concentration of 30% to act as the cryoprotectant in the subsequent data collection step.

A similar procedure was followed to obtain XIP-I-XYNC complex crystal. The *P. funiculosum* xylanase and the inhibitor were mixed together in a 1:1 ratio. The hanging drops consisted of 1 $\mu$l of the protein solution (3.5 mg/ml) together with 1 $\mu$l of the reservoir solution composed of 34% PEG 4000, 0.2 M ammonium sulfate, and 1.5% 1,2,3-heptanetriol. Suitable crystals for data collection were obtained within 3 weeks. The complex crystallized in the space group $P4_32_12$ ($a = b$ = 98.7 Å and $c$ = 109.8 Å).

X-ray diffraction data were collected at 100 K on an ADSC Q4 CCD detector using synchrotron radiation at ID14-EH1 beamline in European Synchrotron Radiation Facility (Grenoble, France) for XIP-I-XLNC crystal and on a MarCCD detector using synchrotron radiation at X06 SA beamline in Swiss Light Source (Villigen, Switzerland) for XIP-I-XYNC crystal. Data processing was performed using the DENZO and SCALEPACK programs (16). Data collection statistics are given in supplemental Table I.

*Structure Determination*—The structure of XIP-I-XLNC complex was solved by molecular replacement using the AMoRe program (17) with XIP-I (Protein Data Bank code 1OMO) and *Penicillium simplicissimum* xylanase (Protein Data Bank code 1BG4) as the search models. The rotation and translation functions gave a unique solution. Before fitting, the correlation coefficient and $R$-factor were 52.6 and 39.3%, respectively, which refined to 60.9 and 36.2%, respectively. CNS (18) and REFMAC (19) refinements were carried out between 20 and 1.7 Å. After performing several cycles of refinement and manual replacement and building on the graphic display with the TURBO-FRODO program (20), the $R$-factor has decreased to 13.3% ($R$-free 16.5%).

The molecular replacement method using the AMoRe program (17) was also used to solve the structure of the XIP-I-XYNC complex. The search model for the enzyme was the structure of *Aspergillus niger* xylanase (Protein Data Bank code 1UKR). The rotation function yielded one solution for the inhibitor but no peak above background for the enzyme. The phased translation function with the known position of XIP-I gave a solution, with a correlation coefficient and an $R$-factor of 41.9 and 46.3%, respectively, for data between 15 and 4 Å. After rigid body refinement, the correlation coefficient was 52.4% with an $R$-factor of 41.8%. The refinement was performed using the TLS option in the program REFMAC (19). After performing several cycles of refinement and manual replacement and building, the $R$-factor decreased to 25.2% ($R$-free 28.9%) for a resolution between 20 and 2.5 Å.

*Coordinates*—The atomic coordinates and structure factors for the XIP-I *A. nidulans* xylanase and XIP-I *P. funiculosum* xylanase complexes have been deposited in the Protein Data Bank (accession codes 1TA3 and 1TE1 for XIP-I-XLNC and XIP-I-XYNC, respectively).

*Structural Alignments*—A first superposition of each molecule on the structure of *A. nidulans* and *P. funiculosum* (for GH10 and GH11, respectively) was performed by using the three C-$\alpha$ atoms of amino acids found in the active site. The superimposition was then refined by using all the C-$\alpha$ pairs that were distant by less than a given cut-off distance. In our strategy, the initial cut-off was 1 Å and 0.5 Å in a second step. The quality of the superposition can be assessed by the number of C-$\alpha$ atoms that are involved in the last calculation step.

## RESULTS AND DISCUSSION

### *Overall Structures*

*Structure of A. nidulans Xylanase (XLNC)*—The *A. nidulans* xylanase displays the typical $(\beta/\alpha)_8$ TIM-barrel fold of GH10 xylanases (Fig. 1*A*). The molecule displays a "salad bowl" shape with an elliptical cross-section at the C-terminal side of the barrel with a maximum shorter and longer axis of 40 and 53 Å, respectively. The three-dimensional structure of XLNC is similar to that of *P. simplicissimum* xylanase XYNA. The architecture of the cleft that runs across the barrel top is characteristic of GH10 xylan-binding sites with the two conserved catalytic residues, Glu-$131_{XLNC}$ and Glu-$239_{XLNC}$ (acid-base catalyst and nucleophile, respectively), facing each other on opposite sides approximately halfway through its length. The major main chain difference between these two enzymes occurs in the loop connecting strand $\beta_6$ to helix $\alpha_6$ which constitutes the surface edge at the distal aglycone region of the substrate binding cleft. In this loop, the segment following the conserved residue His-$209_{XLNC}$ is longer in XLNC, resulting in a significant structural rearrangement at the extremity of the groove. A xylopentaose moiety can easily be modeled into the cleft of XLNC on the basis of the x-ray structure of the *P. simplicissimum* xylanase bound with xylooligosaccharides (Protein Data Bank code 1B3Z) (21).

*Structure of P. funiculosum Xylanase (XYNC)*—The *P. funiculosum* xylanase conforms to the $\beta$-jelly roll fold of other GH11 xylanases (Fig. 1*B*). The conformation of GH11 xylanases has been compared with the shape of a right hand with the "fingers" at the top, the "palm" at the bottom, and the thumb at the right-hand side of the molecule (22). The final model of the enzyme contains 1 $\alpha$-helix and 14 $\beta$-strands forming 2 curved $\beta$-sheets, A and B (Fig. 1*B*). The curved $\beta$-sheet B, the "cord" and the thumb form the cylindrical active site, which is lined with many aromatic amino acid residues. Although the main architecture is conserved, XYNC shows several differences with well characterized xylanases from *A. niger, Bacillus agaradherens,* and *Bacillus circulans* (23–25). In particular, changes are observed in the conformation of the thumb and in the shape of the loop linking strands A2 and B2 of the palm, two regions involved in the interaction with XIP-I (see below). The structural elements of the substrate-binding cleft are similar to other GH11 xylanases, and the catalytic residues, Glu-$86_{XYNC}$ and Glu-$177_{XYNC}$, are invariant. The dimensions of the substrate binding cleft indicates that the enzyme contains three glycone (−3 to −1) and two aglycone (+1 to +2) subsites.

### *Structural Basis for the Inhibition of GH10 and GH11 Xylanases by XIP-I*

*Interaction with GH10 Xylanase*—The structure of the complex between XIP-I and XLNC revealed extensive interactions between the two proteins, resulting in the burial of 1130 Å$^2$ of accessible surface area. The two elliptical TIM barrel scaffolds interact such that the major axes of XIP-I and XLNC are perpendicular (Fig. 1*A*). XIP-I $\alpha_7$ helix (232–245) interacts with the loops forming the xylanase groove through enzyme residues 46–47 (loop $\beta_2$-$\alpha_2$), 87–90 (loop $\beta_3$-$\alpha_3$), 131–146 (loop $\beta_4$-$\alpha_4$), and 269–281 (loop $\beta_8$-$\alpha_8$) (Fig. 2*A*; supplemental Table II). Helix $\alpha_7$ covers the central part of the XLNC substrate binding cleft from subsites −3 to +2, resulting in the occlusion of the active site of the enzyme. Side chains emerging from the helix point into the heart of the cleft and occupy the four central subsites: −1 (Lys-$234_{XIP\text{-}I}$), +1 (Asn-$235_{XIP\text{-}I}$), +2 (His-$232_{XIP\text{-}I}$), and −2 (Tyr-$238_{XIP\text{-}I}$), whereas Lys-$246_{XIP\text{-}I}$ sterically blocks access to subsite −3. Lys-$234_{XIP\text{-}I}$ makes a direct hydro-

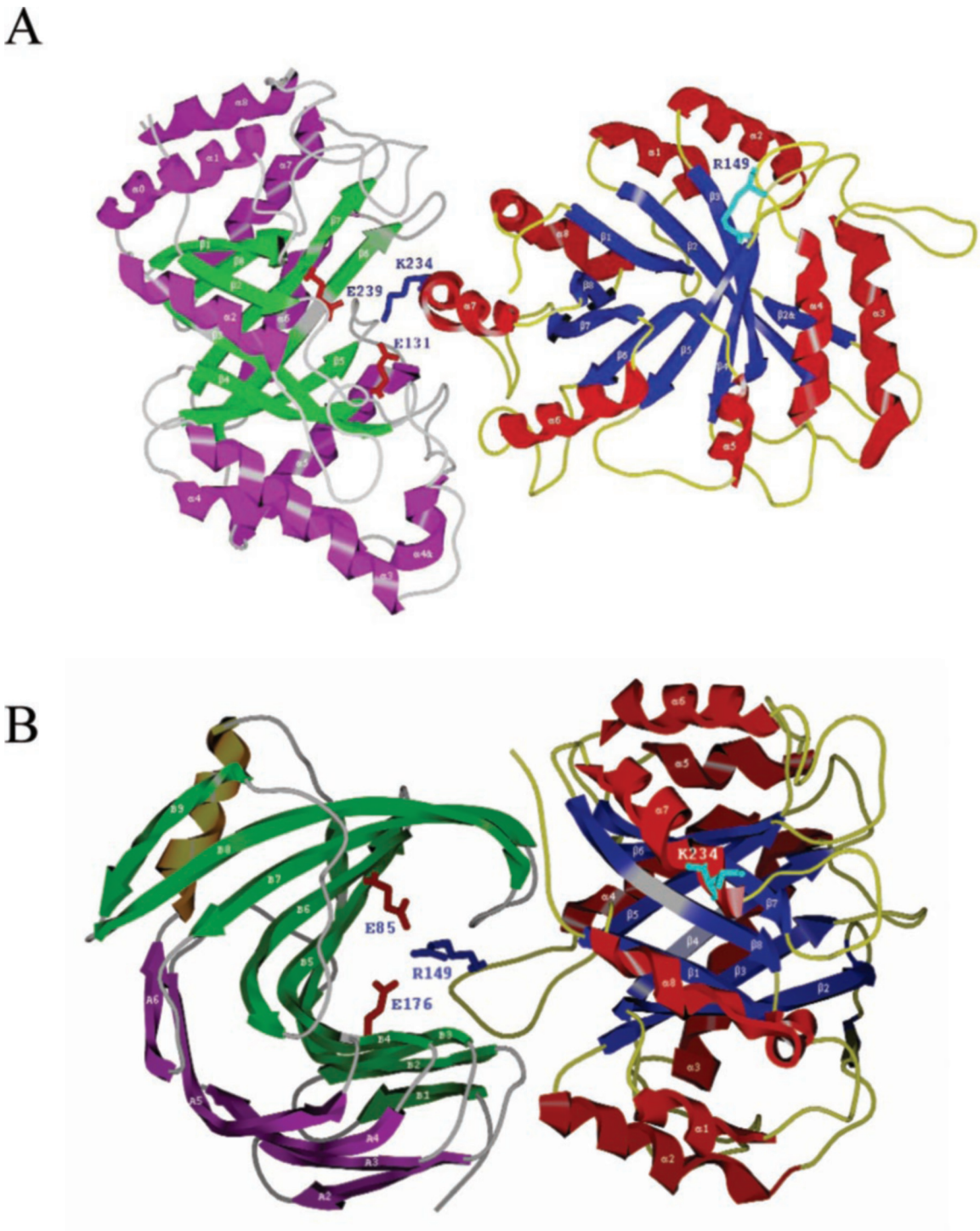


FIG. 1. *A*, structure of the XIP-I-XLNC complex. XIP-I is in *red* and *blue*, and *A. nidulans* xylanase (XLNC) is in *purple* and *green.* The main interaction residues are shown in a *stick* representation, Lys-234$_{XIP-I}$ side chain (*dark blue*) is important for the interaction with XLNC, and Arg-149$_{XIP-I}$ (*light blue*) is important for the interaction with XYNC (*B*), together with the side chains of the two catalytic residues (*red*). *B*, structure of the XIP-I-XYNC complex. XIP-I is in *red* and *blue*, and *P. funiculosum* xylanase (XYNC) is in *purple* and *green.* The long inhibitor loop interacting directly in the xylanase active site is shown. The main interaction residues are shown in a *stick* representation, Arg-149$_{XIP-I}$ side chain (*dark blue*) is important for the interaction with XYNC, and Lys-234$_{XIP-I}$ (*light blue*) is important for the interaction with XLNC (see *A*), together with the side chains of the two catalytic residues (*red*). Figures were generated by SPOCK (36).

gen bond with the acid-base catalyst Glu-131$_{XLNC}$ and water-mediated hydrogen bonds with the nucleophile Glu-239$_{XLNC}$. In the complex, the heart of the substrate binding site is occupied by an aromatic cluster of residues from the inhibitor (Tyr-237$_{XIP-I}$, Tyr-238$_{XIP-I}$, His-232$_{XIP-I}$, Trp-230$_{XIP-I}$, and Tyr-273$_{XIP-I}$) and the enzyme (Trp-269$_{XLNC}$, His-209$_{XLNC}$, Trp-277$_{XLNC}$, Tyr-174$_{XLNC}$, and Arg-278$_{XLNC}$). In the structure of XYNA in complex with xylopentaose (Protein Data Bank code 1B3Z), Trp-276$_{XYNA}$ forms a "lid" over the active site and stacks with the xylose ring bound at subsite −1 (21). In the XIP-I-XLNC complex, the corresponding residue (Trp-277$_{XLNC}$) is displaced upon inhibitor binding by the helical inhibitory head, confirming the flexibility of the tryptophan "above" the −1 subsite (5). The movement of Trp-277$_{XLNC}$ is accompanied by a rearrangement of the adjacent Arg-278$_{XLNC}$; both residues are very well defined in the electron density. Within the "product

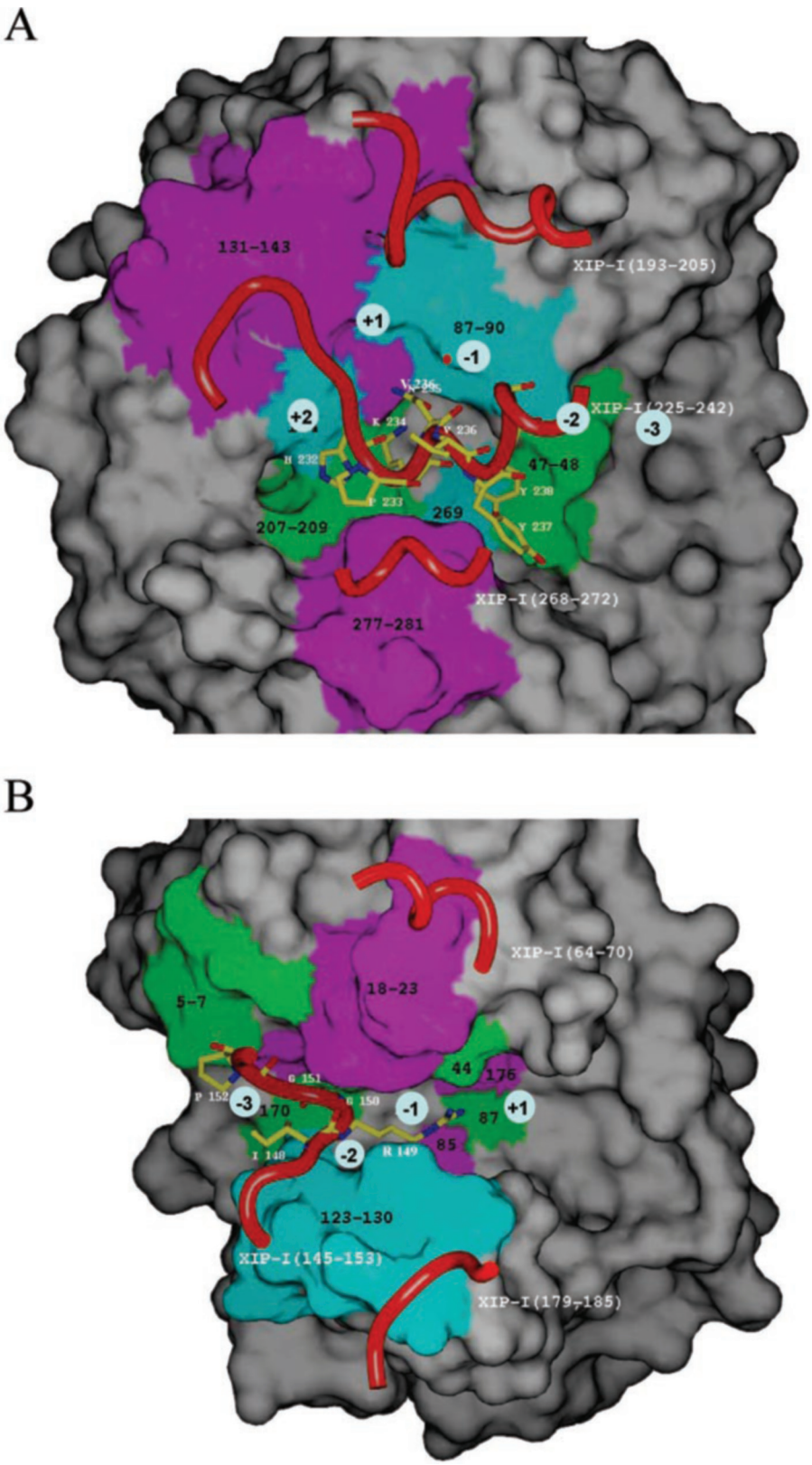


FIG. 2. *A,* structural basis for the inhibition of GH10 xylanase XLNC. The molecular surface of XLNC is shown in *gray*. Enzyme surfaces (and corresponding residues numbering) interacting with XIP-I are depicted in *purple*, *blue*, and *green*. The known substrate subsites are labeled. Inhibitor residues interacting in the active site groove are shown in a *stick* representation (colored according to the atom type). Regions from the inhibitor molecule involved in the inhibiting mechanism are represented by *red tubes* (residue numbering in *parentheses*). *B*, structural basis for the inhibition of GH11 xylanase XYNC. A close up of the XYNC active site is the same as in *A*. Figures were prepared with SPOCK (36).

release area" (subsites +1 to +2) of the xylanase cleft, a tyrosine side chain (Tyr-175$_{XYNA}$) stacks against the xylobiose entity bound to subsites +1 through +2 (21); in the XIP-I-XLNC complex, the corresponding tyrosine residue (Tyr-174$_{XLNC}$) interacts with the side chain of His-232$_{XIP\text{-}I}$ occupying subsite +2, mimicking substrate enzyme recognition at the +2 subsite.

*Interaction with GH11 Xylanase*—In the XIP-I-XYNC complex, there are extensive interactions between the two proteins, with a contact surface area of 870 Å$^2$. A Π-shaped long loop from XIP-I protrudes between the thumb and the palm of the enzyme (Fig. 1*B*), blocking access to the active site; this interaction is associated with tight interaction with the thumb and the facing palm regions including segments from the strands of the curved $\beta$-sheet B and the loop A2B2 (Fig. 2*B*). The primary contact region in XIP-I involves residues 148–154 from the Π-shaped L$\alpha_4\beta_5$ loop and interacts with residues from the

enzyme active center (region 1), the thumb (region 2), and the palm of the enzyme (region 3) (supplemental Table III). The loop is sited in the mouth of the active site cylinder, blocking access to the three glycone subsites. The top of the inhibitor loop is slightly twisted, allowing the 150–152 (Gly-Gly-Pro) segment to extend closely parallel to the −3 subsite plane, whereas the main chain segment 149–150 occupies subsite −2 (Fig. 2*B*). The carbonyl main chain of Gly-$150_{XIP\text{-}I}$ interacts with Ser-$16_{XYNC}$, a residue that is predicted to interact with sugar units bound to the glycone subsites (24, 25). The planar side chain of Arg-$149_{XIP\text{-}I}$ emerging from the left edge of the loop, in turn, extends into the −2 and −1 subsites; its hydrophobic part stacks against Trp-$18_{XYNC}$, a residue highly conserved throughout GH11 (mimicking stacking of the substrate xylose ring located at the −2 subsite) (5, 24). The guanidinium group of Arg-$149_{XIP\text{-}I}$, which points into the crucial subsite −1, hydrogen-bonds with the catalytic acid-base Glu-$176_{XYNC}$ and Tyr-$87_{XYNC}$. Most interesting, an arginine residue in the microbial inhibitor tendamistat forms a salt bridge to the acid-base catalyst of the porcine pancreatic $\alpha$-amylase, resulting in the inactivation of the glycoside hydrolase (26), a feature which might recurs in other glycosidase-inhibitor complexes. In the present structure, the $NH_2$ atom of Arg-$149_{XIP\text{-}I}$ is in the equivalent position to the activated solvent molecule that acts as the nucleophile in the hydrolysis of the glycosyl-enzyme intermediate in the *B. circulans* xylanase (24), and it establishes an analogous hydrogen-bonding pattern with the catalytic acid-base and adjacent Tyr-$87_{XYNC}$. The same characteristic feature was observed in the inhibition of pancreatic $\alpha$-amylase by the proteinaceous bean inhibitor from *Phaseolus vulgaris* where the hydroxyl group of Tyr-$37_{inhibitor}$ makes a strong hydrogen bond to the acid-base catalyst, replacing the intervening water molecule (27).

In addition to the enzyme active site cleft (region 1), neighboring regions are in tight contact with XIP-I (Fig. 2*B*), which includes an interaction between the thumb of XYNC (region 2) and three regions of XIP-I: the inhibitory loop and loops $\alpha_5\beta_6$ and $\alpha_6\beta_7$. This is consistent with site-directed mutagenesis studies demonstrating that the equivalent residue to Asn-$123_{XYNC}$ in the *A. niger* xylanase thumb plays a key role in the interaction with XIP-I (13). The final enzyme region (region 3) consists of segments from strands B1, B2, and B3 facing the Π-shaped inhibitor loop (residues 5–7, 16–20, and 44) and the loop $B_2A_2$ (residues 21–23) and its neighboring region (residues 41–43), which interact with the C-terminal extremity of XIP-I helix $\alpha$2.

These protein complexes show that GH10 and GH11 xylanases interact with distinct regions of XIP-I, allowing a possible simultaneous binding of the inhibitor to both target enzymes (Fig. 3).

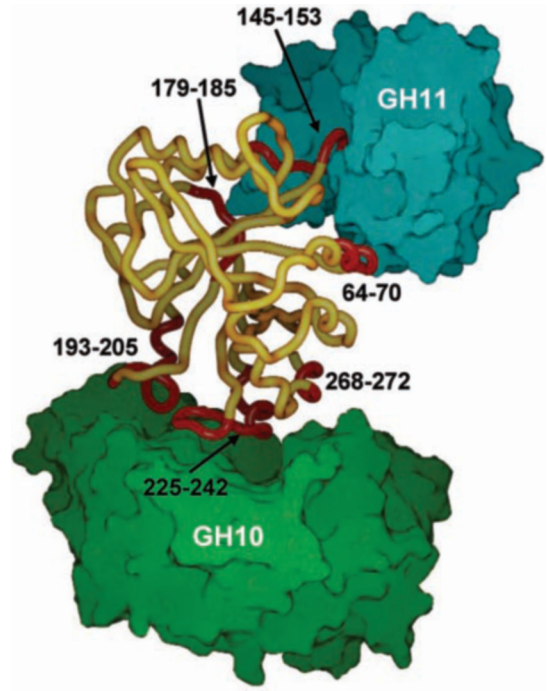


FIG. 3. **A model of the ternary complex between XIP-I (in *yellow*) and two glycoside hydrolases, XLNC (GH10 xylanase, in *green*) and XYNC (GH11 xylanase, in *blue*).** Regions from the inhibitor molecule involved in the inhibiting mechanism are represented by *red tubes*. Modeling was based on the present coordinates (via superimposition of the XIP-I part). Figure was prepared with SPOCK (36).

### *Determinants of Specificity of XIP-I*

Kinetic studies have established that XIP-I is a strong inhibitor of fungal GH10 and GH11 xylanases but does not inhibit any of the bacterial xylanases tested (10). The resolution of the three-dimensional structures of the xylanase-inhibitor complexes has identified the major structure features of these enzymes that are recognized by XIP-I. These data can be used to predict which bacterial and fungal xylanases will be inhibited by XIP-I. The validation of this prediction strategy is outlined below.

*Specificity for GH10 Xylanases*—The interaction of GH10 *A. nidulans* xylanase with XIP-I occurs through loops $\beta_2$-$\alpha_2$ (residues 46–47), $\beta_3$-$\alpha_3$ (residues 87–90), $\beta_4$-$\alpha_4$ (residues 131–146), and $\beta_8$-$\alpha_8$ (residues 269–281), located around the enzyme active site. The crystal structures of two fungal and six bacterial GH10 xylanases have been reported. Comparison of the *fungal* structures with XLNC in complex with XIP-I does not reveal any significant structural differences in the loop regions located around the active site and the regions corresponding to the interface with the inhibitor. In sharp contrast, the structures of the *bacterial* xylanases revealed insertions in the $\beta/\alpha$-loop segments at the carboxyl side of the $\beta$-barrel, which interact with XIP-I in XLNC. The location of these insertions varies with the xylanase (Fig. 4*A*). Among the bacterial xylanases of known three-dimensional structures, only Xyn10A from *Pseudomonas fluorescens* (*Cellvibrio japonicus*) (1CLX) was tested against XIP-I and was shown not to be inhibited (10). The lack of inhibition of this xylanase is explained by the insertions in loops $\beta_4$-$\alpha_4$ (residues 134–138) and $\beta_8$-$\alpha_8$ (residues 269–281) of the enzyme, which would prevent binding of XIP-I by steric hindrance. A similar insertion in *Cellulomonas fimi* (Protein Data Bank code 1EXP) and *Clostridium thermocellum* (Protein Data Bank code 1XYZ) xylanases would also predict a lack of inhibition for these enzymes. This hypothesis is in agreement with the findings that all the fungal GH10 xylanases evaluated were inhibited by XIP-I, apart from that of *Aspergillus aculeatus* (10). The lack of inhibition of this fungal enzyme is consistent with two large insertions after $\beta$-strands 7 and 8, as observed in the *C. fimi* and *C. thermocellum* xylanases. However, such structural differences are less obvious for other bacterial xylanases of known three-dimensional structure such as those from *Streptomyces lividans* (Protein Data Bank code 1EOV) and *Streptomyces olivaceoviridis* (Protein Data Bank code 1ISV). A search for interface-forming residues significantly different from the *A. nidulans* xylanase highlighted a stretch of amino acids around position 280 (loop $\beta_8/\alpha_8$) of the *S. lividans* enzyme in which two residues positioned at the interface (Ser and Asp in *A. nidulans* xylanase) are replaced by amino acids with longer side chains (Glu and Gln) that are likely to make steric clashes with XIP-I. This sequence

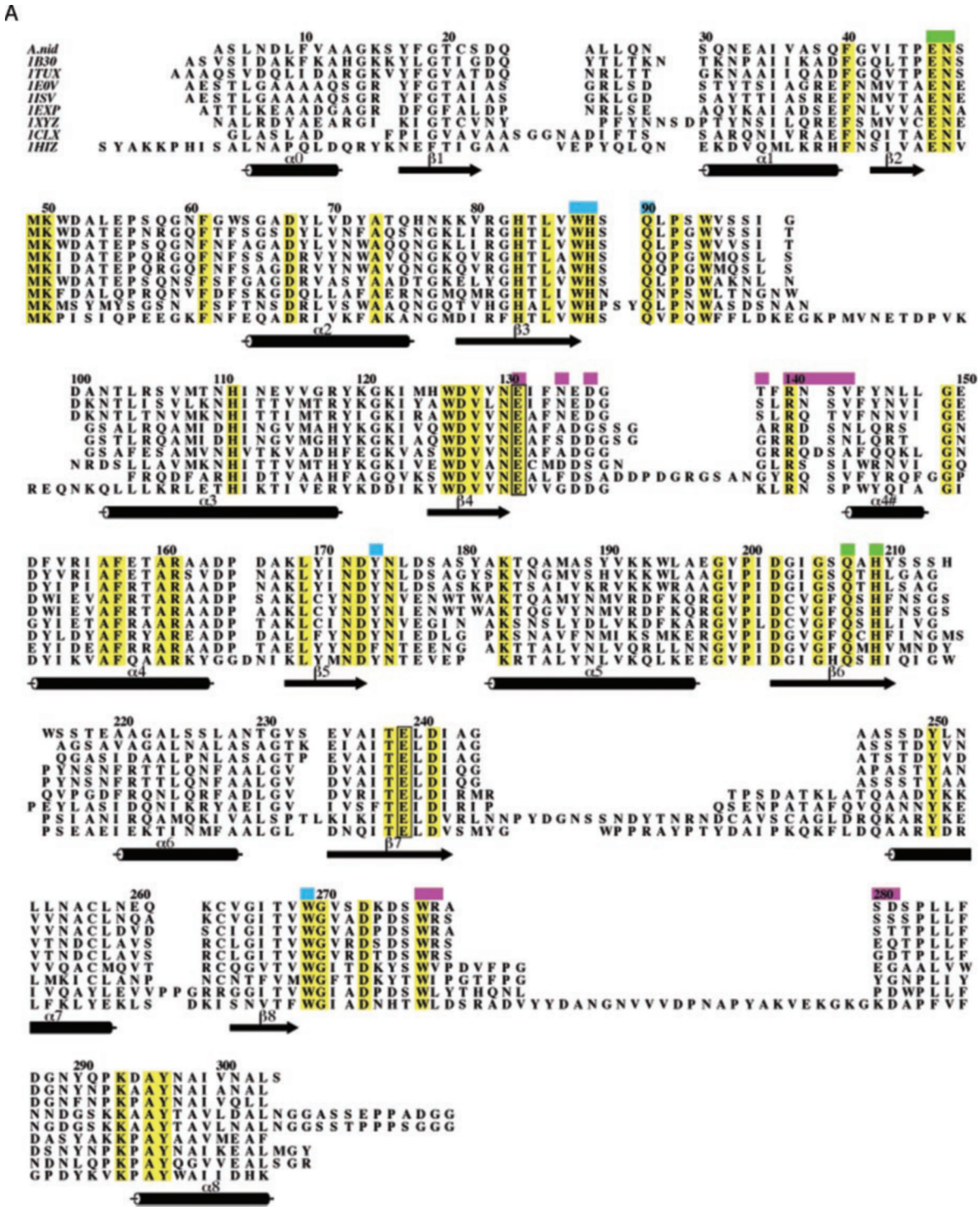


FIG. 4. **Multiple structural alignments of xylanases from related species.** The sequences are referenced with the corresponding Protein Data Bank code (the *letter B* before the Protein Data Bank code indicates a bacterial origin). The regions of interaction are depicted in *purple, blue,* and *green*, as in Fig. 2. Highly conserved residues are in *yellow*. Figure was prepared with Alscript (37). *A,* structural alignment of XLNC from *A. nidulans* (*A.nid*) with GH10 xylanases. They include two fungal enzymes from *P. simplicissimum* (1B30) and *Thermoascus aurantiacus* (1TUX) and six bacterial enzymes from *S. lividans* (B1EOV), *S. olivaceoviridis* (B1ISV), *C. fimi* (B1EXP), *C. thermocellum* (B1XYZ), *P. fluorescens cellulosa* (*C. japonicus*) (B1CLX), and *Geobacillus stearothermophilus* (B1HIZ). *B,* structural alignment of XYNC from *P. funiculosum* (*P.fun*) with GH11 xylanases. They include eight fungal enzymes from *Trichoderma harzianum* (1XND), *Trichoderma reesei* (xylanase 2, 1ENX), *Paecilomyces varioti bainier* (1PVX), *Thermomyces lanuginosus* (1YNA), *Chaetomium thermophilum* (1H1A), *A. niger* (1UKR), *Aspergillus kawachii* (1BK1), and *T. reesei* (xylanase 1, 1XYN), and seven bacterial enzymes from *Actinomadura flexuosa* (B1M4W), *Streptomyces* sp. *S38* (B1HIX), *B. agaradhaerens* (B1H4G), *B. subtilis* (B1IGO), *Dictyoglomus thermophilum* (B1F5J), *B. circulans* (B1BCX), and *B. subtilis* (B1AXK).

difference is absent from the corresponding region of the *S. olivaceovirdis* xylanase, suggesting that this prokaryotic xylanase could be inhibited by the wheat protein and thus questions whether XIP-I binds exclusively to fungal xylanases. Phylogenetic analyses have shown that GH10 xylanases can be further divided into two clusters; one containing fungal enzymes only and the other including enzymes from both bacteria and fungi (28). The sequences of the fungal xylanases from

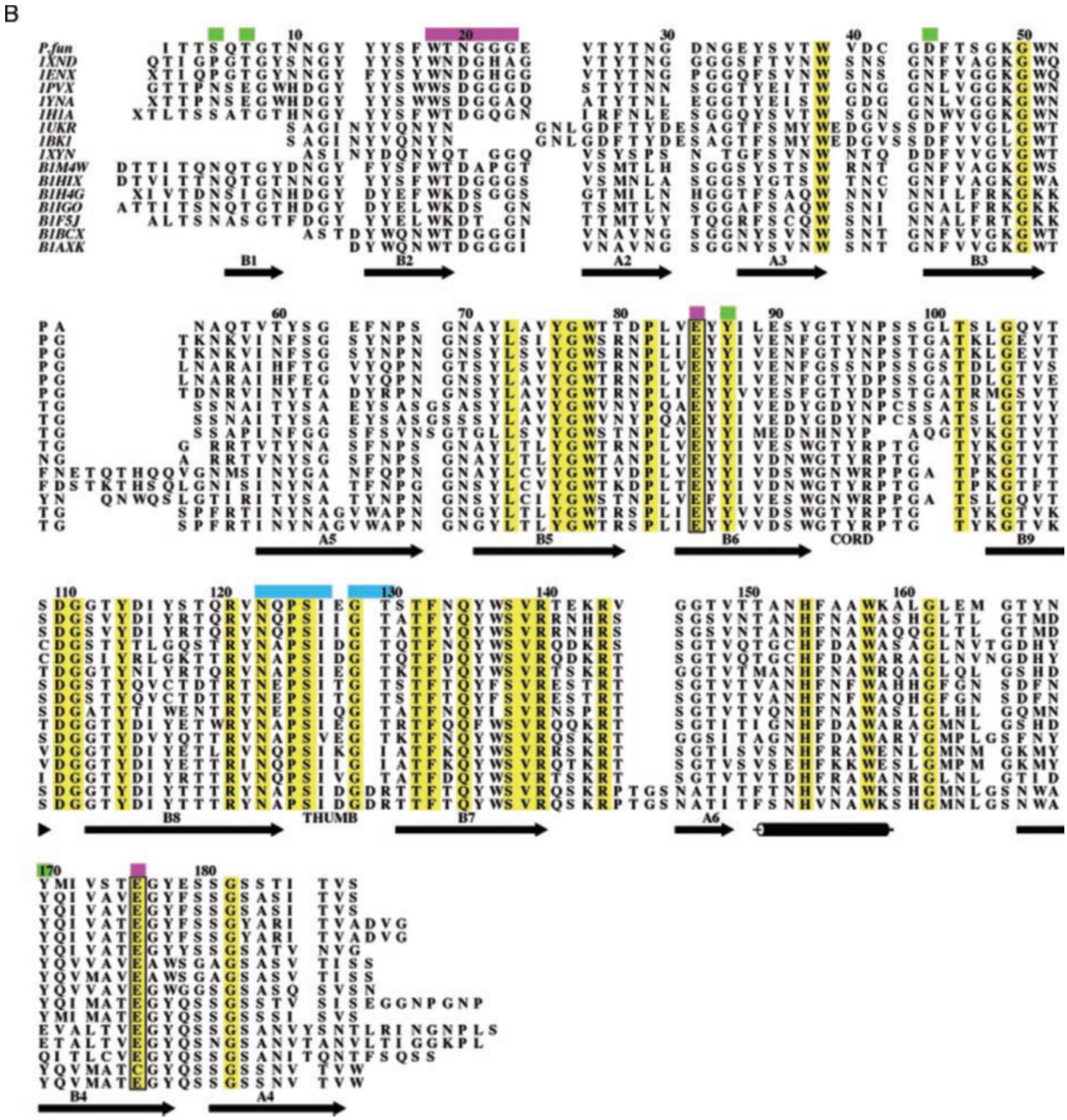


FIG. 4—*continued*

*Agaricus bisporus*, *Humicola grisea,* and *Filobasidium floriforme* are closely related to the bacterial xylanase from *C. fimi* and show a 5-amino acid insertion in the $\beta_8$-$\alpha_8$ loop (compared with XLNC), which would prevent XIP-I binding. Thus, XIP-I does not appear to display absolute specificity for fungal xylanases but is likely to target GH10 enzymes that lack the extended loops at the carboxyl side of the $\beta$-barrel. The physiological role of XIP-I is not known; the protein may contribute to plant defense, by inhibiting pathogen-derived xylanases, or play a role in plant metabolism by preventing the remodeling of plant cell walls during specific phases of plant development. The only wheat xylanase characterized to date belongs to GH10, and sequence alignment reveals insertions in recognition loops that would make steric clashes with the inhibitor. This is consistent with the detection of endogenous xylanase activity in wheat grains and the observation that XIP-I does not inhibit this activity *in vitro* (29). The structural data thus seem to support a role for XIP-I in plant defense. It might be that the inhibitor has evolved to deal with a specific pathogen whose xylanases do not contain these loops; however, this cannot be confirmed as the sequences of xylanases from known wheat pathogens have not been reported.

*Specificity for GH11 Xylanases*—The XIP-I strategy for inhibition of GH11 xylanases consists of an inhibitory head (the Π-shaped loop 148–153) blocking the entrance to the active site groove. The main inhibition determinant involves a functional arginine side chain projecting into the glycone subsites of the active site of the enzyme. Interactions with regions of the XYNC (thumb and palm) surrounding the entrance of the active site groove are also important recognition determinants for XIP-I, with the overall shape and amino acid composition of the thumb playing a particularly important role in inhibitor binding. The structural alignment of XYNC with GH11 xylanases with known three-dimensional structures (eight fungal and six bacterial enzymes) showed insertions in the region surrounding the tip of the thumb at the highly conserved residue Gly-$129_{XYNC}$ in several enzymes (Fig. 4*B*). Kinetic studies have established that XIP-I is a strong inhibitor of a number of

fungal but not bacterial GH11 xylanases (10). The lack of inhibition of the *Bacillus subtilis* xylanase can be explained by the insertion of an Asp at position 129 and the replacement of the following threonine by an arginine ($^{128}$EG-**T**$^{130}{}_{XYNC}$ → $^{275}$DG**DR**$^{278}{}_{1AXK}$). The superimposition of the *B. subtilis* xylanase structure with that of XYNC (in complex with XIP-I) shows that the insertion would cause this loop to adopt a strikingly different conformation that would introduce steric clashes with XIP-I (see Fig. 2*B*), thus preventing inhibitor binding. This hypothesis is further supported by the lack of inhibition by XIP-I of a fungal GH11 xylanase from *Neocallimastix patriciarum* (GenBank™ accession number X65526), which contains an insertion after Gly-129$_{XYNC}$.[2] The insertion in the tip region is also observed in the xylanase from *B. circulans* (Protein Data Bank code 1BCX) and is thus predicted not to be inhibited by XIP-I. However, a different situation occurs for the *B. agaradhaerens* xylanase (Protein Data Bank code 1H4H), a bacterial enzyme not inhibited by XIP-I (10). Although the overall conformation of the thumb region is similar to that of XYNC without any insertion in the tip region, a search for interface-forming residues highlighted a significant difference between the enzymes: $^{128}$EG**T**S$^{131}$ in XYNC is replaced by $^{136}$KG**I**A$^{139}$ in the *B. agaradhaerens* xylanase. The Ile side chain (instead of Thr) is predicted to clash against Asn-147$_{XIP\text{-}I,}$ emerging from the inhibitory loop, leading to a weak interaction in this area. In addition, it is likely that the hydrogen bond formed between Asn-147$_{XIP\text{-}I}$ and Thr-130$_{XYNC}$ would not occur between the *B. agaradhaerens* enzyme and the inhibitor. It is worth noting that Thr-130$_{XYNC}$ is highly conserved in GH11 xylanases. The lack of inhibition of *B. agaradhaerens* xylanase can also be due to differences in the loop B2A2, another region involved in the interaction with XIP-I; the amino acid sequence $^{20}$N**G**GG$^{23}$ in XYNC is replaced by $^{21}$D**S**GG$^{24}$ in the *B. agaradhaerens* xylanase. The glycine-rich sequence in XYNC may confer flexibility to this segment, whereas the Ser-22 in the *B. agaradhaerens* enzyme might restrict and/or alter the conformation of the loop. This predicted lack of flexibility in the *B. agaradhaerens* enzyme may cause steric clashes with the inhibitor interacting area including the C-terminal extremity of XIP-I helix $\alpha_2$. Among the fungal xylanases tested, the *A. niger* xylanase (Protein Data Bank code 1UKR) is the only one for which a three-dimensional structure is available. The conformation of the *A. niger* xylanase thumb is similar to that of XYNC without any insertion in the tip region. However, there are two striking structural differences with XYNC as follows: (i) the strand B1 is absent from the *A. niger* enzyme, and (ii) the loop region $B_2A_2$ (residues 21–23) of the *A. niger* xylanase is two residues shorter than in XYNC and adopts a very different conformation. This is likely to cause a weaker interaction, explaining the tighter binding of XIP-I to XYNC ($K_i$ of 3.4 nM) compared with the *A. niger* xylanase ($K_i$ of 350 nM) (10). This confirms that, although inhibition of GH11 xylanases by XIP-I is centered on a single loop interacting in the active site, tight binding is mediated by recognition of neighboring regions of the enzyme. The finding that some fungal GH11 xylanases are not inhibited by XIP-I reinforces our suggestion that XIP-I does not display absolute specificity for fungal xylanases. In terms of molecular evolution, the fungal xylanases which, based on the present structural data, are predicted not to be inhibited by XIP-I are those produced by anaerobic fungi (*e.g. Neocallimastix*), which play a significant role in the degradation of plant hemicellulose, the most abundant nutrient in the rumen. In a recent classification (30), fungal GH11 xylanases are divided into three groups I, II, and III. The enzymes in groups I and II are mostly the 20-kDa enzymes of basic and acidic pI, respectively (30). The xylanases from *P. funiculosum* and *A. niger*, both inhibited by XIP-I, belong to groups I and II, respectively, whereas the anaerobic fungal xylanases belong to group III along with the xylanase from the rumen bacterium *Fibrobacter succinogenes,* which is uninhibited by XIP-I (10). There is a very strong similarity between different rumen fungal and bacterial glycoside hydrolases, which is believed to have occurred through horizontal gene transfer events (31).

*Conclusions*—This study shows how the peptide backbone and side chains of the wheat proteinaceous inhibitor XIP-I mimic the interaction of xylanases with oligosaccharides and occlude the active site. The inhibition strategy is novel in that XIP-I binds to two glycoside hydrolases that display a different fold at distinct locations. Substrate mimicry in the active site is a key element of the inhibition mechanism of both GH10 and GH11 xylanases. However, XIP-I specificity depends on the details of the architecture of the areas delineating the substrate binding groove that vary significantly between enzymes from the same family. The structural predictions (supported by the available biochemical data) indicating that XIP-I is able to inhibit xylanases from both fungal and bacterial origin but not the corresponding wheat enzymes support the hypothesis that the inhibitor protects the grain from pathogen attack. The structure of XIP-I resembles GH18 chitinases. Plant chitinases are "pathogenesis-related proteins" that exhibit rapid evolution by acting as prime targets for the co-evolution of plant-pathogen interactions (32), and it is tempting to speculate that the novel function of XIP-I emerged from a class of proteins that was already overexpressed in response to pathogen attack. The intricate recognition specificities of XIP-I toward specific xylanases from both GH10 and GH11 families might be the result of plant evolution to counteract the many xylanases secreted by bacteria and fungi, similar to polygalacturonase-inhibiting proteins (33). This could also explain why two different classes of xylanase inhibitors with different specificities and expression patterns occur in cereals (29, 34). TAXI is the other type of xylanase inhibitor isolated from wheat and is specific for GH11 xylanases (35). Both inhibitors show a common inhibition strategy by binding to the active site region (Sansen *et al.*) (38). The different specificities displayed by TAXI-I and XIP-I might be indicative of a distinct role in plant defense depending on the part of the plant that is affected by the infection, the stage in plant development, and the type of pathogens or nature of the isozyme secreted by a pathogen.

*Acknowledgments*—We thank European Synchrotron Radiation Facility and Swiss Light Source for beam time allocation.

REFERENCES

1. Coutinho, P. M. & Henrissat, B. (1999) in *Recent Advances in Carbohydrate Bioengineering* (Gilbert, H. J., Davies, G. J., Henrissat, B., and Svensson, B., eds) pp. 3–12, Royal Society of Chemistry, Cambridge, UK
2. Kulkarni, N., Shendye, A. & Rao, M. (1999) *FEMS Microbiol. Rev.* **23,** 411–456
3. Jeffries, T. W. (1996) *Curr. Opin. Biotechnol.* **7,** 337–342
4. Biely, P., Vrsanska, M., Tenkanen, M. & Kluepfel, D. (1997) *J. Biotechnol.* **57,** 151–166
5. Sabini, E., Sulzenbacher, G., Dauter, M., Dauter, Z., Jorgensen, P. L., Schulein, M., Dupont, C., Davies, G. J. & Wilson, K. S. (1999) *Chem. Biol.* **6,** 483–492
6. Ducros, V., Charnock, S. J., Derewenda, U., Derewenda, Z. S., Dauter, Z., Dupont, C., Shareck, F., Morosoli, R., Kluepfel, D. & Davies, G. J. (2000) *J. Biol. Chem.* **275,** 23020–23026
7. Juge, N., Payan, F. & Williamson, G. (2004) *Biochim. Biophys. Acta* **1696,** 203–211
8. Gebruers, K., Brijs, K., Courtin, C. M., Fierens, K., Goesaert, H., Rabijns, A., Raedschelders, G., Robben, J., Sansen, S., Sorensen, J. F., Van Campenhout, S. & Delcour, J. A. (2004) *Biochim. Biophys. Acta* **1696,** 213–221
9. McLauchlan, W. R., Garcia-Conesa, M. T., Williamson, G., Roza, M., Ravestein, P. & Maat, J. (1999) *Biochem. J.* **338,** 441–446
10. Flatman, R., McLauchlan, W. R., Juge, N., Furniss, C., Berrin, J. G., Hughes, R. K., Manzanares, P., Ladbury, J. E., O'Brien, R. & Williamson, G. (2002) *Biochem. J.* **365,** 773–781

[2] A. Durand and H. J. Gilbert, personal communication.

11. Furniss, C. S. M., Belshaw, N. J., Alcocer, M. J., Williamson, G., Elliott, G. O., Gebruers, K., Haigh, N. P., Fish, N. M. & Kroon, P. A. (2002) *Biochim. Biophys. Acta* **1598,** 24–29
12. Payan, F., Flatman, R., Porciero, S., Williamson, G., Juge, N. & Roussel, A. (2003) *Biochem. J.* **372,** 399–405
13. Tahir, T. A., Berrin, J. G., Flatman, R., Roussel, A., Roepstorff, P., Williamson, G. & Juge, N. (2002) *J. Biol. Chem.* **277,** 44035–44043
14. MacCabe, A. P., Fernandez-Espinar, M. T., de Graaff, L. H., Visser, J. & Ramon, D. (1996) *Gene* (*Amst.*) **175,** 29–33
15. Belshaw, N. J., Haigh, N. P., Fish, N. M., Archer, D. B. & Alcocer, M. J. (2002) *Appl. Microbiol. Biotechnol.* **60,** 455–460
16. Otwinowski, Z. & Minor, W. (1997) *Methods Enzymol.* **276,** 307–326
17. Navaza, J. (1994) *Acta Crystallogr. Sect. A* **50,** 157–163
18. Brunger, A. T., Adams, P. D., Clore, G. M., DeLano, W. L., Gros, P., Grosse-Kunstleve, R. W., Jiang, J. S., Kuszewski, J., Nilges, M., Pannu, N. S., Read, R. J., Rice, L. M., Simonson, T. & Warren, G. L. (1998) *Acta Crystallogr. Sect. D Biol. Crystallogr.* **54,** 905–921
19. Collaborative Computational Project Number 4 (1994) *Acta Crystallogr. Sect. D Biol. Crystallogr.* **50,** 760–763
20. Roussel, A. & Cambillau, C. (1991) *Silicon Graphics Geometry Partners Directory,* pp. 86, Silicon Graphics, Mountain View, CA
21. Schmidt, A., Gubitz, G. M. & Kratky, C. (1999) *Biochemistry* **38,** 2403–2412
22. Torronen, A., Harkki, A. & Rouvinen, J. (1994) *EMBO J.* **13,** 2493–2501
23. Krengel, U. & Dijkstra, B. W. (1996) *J. Mol. Biol.* **263,** 70–78
24. Sidhu, G., Withers, S. G., Nguyen, N. T., McIntosh, L. P., Ziser, L. & Brayer, G. D. (1999) *Biochemistry* **38,** 5346–5354
25. Sabini, E., Wilson, K. S., Danielsen, S., Schulein, M. & Davies, G. J. (2001) *Acta Crystallogr. Sect. D Biol. Crystallogr.* **57,** 1344–1347
26. Wiegand, G., Epp, O. & Huber, R. (1995) *J. Mol. Biol.* **247,** 99–110
27. Bompard-Gilles, C., Rousseau, P., Rouge, P. & Payan, F. (1996) *Structure* (*Lond.*) **4,** 1441–1452
28. Sato, Y., Niimura, Y., Yura, K. & Go, M. (1999) *Gene* (*Amst.*) **238,** 93–101
29. Elliott, G. O., McLauchlan, W. R., Williamson, G. & Kroon, P. A. (2003) *J. Cereal Sci.* **37,** 187–194
30. Sapag, A., Wouters, J., Lambert, C., de Ioannes, P., Eyzaguirre, J. & Depiereux, E. (2002) *J. Biotechnol.* **95,** 109–131
31. Garcia-Vallve, S., Romeu, A. & Palau, J. (2000) *Mol. Biol. Evol.* **17,** 352–361
32. Bishop, J. G., Dean, A. M. & Mitchell-Olds, T. (2000) *Proc. Natl. Acad. Sci. U. S. A.* **97,** 5322–5327
33. De Lorenzo, G. & Ferrari, S. (2002) *Curr. Opin. Plant Biol.* **5,** 295–299
34. Fierens, K., Brijs, K., Courtin, C. M., Gebruers, K., Goesaert, H., Raedschelders, G., Robben, J., Van Campenhout, S., Volckaert, G. & Delcour, J. A. (2003) *FEBS Lett.* **540,** 259–263
35. Gebruers, K., Debyser, W., Goesaert, H., Proost, P., Van Damme, J. & Delcour, J. A. (2001) *Biochem. J.* **353,** 239–244
36. Christopher, J. A. (1998) *SPOCK: The Structural Properties Observation and Calculation Kit Program Manual*, Center for Macromolecular Design & Texas A & M University, College Station, TX
37. Barton, G. J. (1993) *Protein Eng.* **6,** 37–40
38. Sansen, S., De Ranter, C. J., Gebruers, K., Brijs, K., Courtin, C. M., Delcour, J. A. & Rabijns, A. (2004) *J. Biol. Chem.* **279,** 36022–36028